



Novel solid polymer electrolyte based on PMMA:CH₃COOLi effect of salt concentration on optical and conductivity studies

Sravanthi Kurapati¹ · Sunita Sundari Gunturi¹ · Krishna Jyothi Nadella¹ · Harikrishna Erothu² 

Received: 26 September 2018 / Revised: 30 November 2018 / Accepted: 10 December 2018 /
Published online: 1 January 2019
© Springer-Verlag GmbH Germany, part of Springer Nature 2019

Abstract

Novel solid polymer electrolyte (SPE) films based on poly(methyl methacrylate) (PMMA) and lithium acetate (CH₃COOLi) with different weight ratios of PMMA:CH₃COOLi wt% (60:40, 70:30, 80:20 wt%) were prepared by solution casting technique. XRD analysis confirmed the amorphous nature of Li–PMMA SPE films. FTIR analysis revealed the structural changes in polymer by complexation with Li salt. From the optical absorbance studies, the value of lowest energy band gap was found to be 3.06 eV for the composition, PMMA:CH₃COOLi (60:40 wt%). From AC impedance studies, the highest value of ionic conductivity 8.21×10^{-5} S/cm at 303 K for the SPE film PMMA:CH₃COOLi (60:40 wt%) is observed compared to the reported literature. From the results of Li–PMMA SPE film with high ionic conductivity, it is a promising material for the application of solid-state battery.

Keywords Li–PMMA SPE · Ionic conductivity · Band gap · Dielectric measurements

Introduction

Increasing global energy consumption over the past decade has created a huge demand for safe and alternative energy sources. Extensive research has been done to address and develop best alternative energy sources. Battery is one of the best

✉ Sunita Sundari Gunturi
physics.ss@gmail.com

✉ Harikrishna Erothu
harikrishnaiitm@gmail.com

¹ Department of Physics, Koneru Lakshmaiah Education Foundation (KLEF), Vaddeswaram, Guntur, Andhra Pradesh 522502, India

² Centre for Advanced Energy Studies (CAES), Koneru Lakshmaiah Education Foundation (KLEF), Vaddeswaram, Guntur, Andhra Pradesh 522502, India

alternative energy sources due to its high energy density and characteristics like low cost, easy to handle, lightweight and eco-friendly in nature [1–5]. Besides electrodes, electrolyte plays a major role in a battery due to its conductive behavior through mobility of ions during charging and discharging. Rechargeable batteries can be classified in many ways based on their physical structure and nature of electrolyte and electrodes. Li-ion batteries (LIBs) are considered to be the best among all the rechargeable batteries due to its outstanding cycle life and cell voltage [6, 7]. Using liquid electrolytes which conduct through lithium ions can lead to short circuit, cell leakage, corrosion, increase in weight and the danger of catching flames. To overcome these complications, Armand et al. [8] introduced polymer electrolytes for the first time. In LIBs, liquid electrolytes have been replaced by solid polymer electrolytes (SPEs) due to improved safety, efficiency, stability and high energy density. These salient features of SPEs have triggered extensive research in the preparation of solvent-free polymer electrolytes for application in energy storage devices like fuel cells, sensors, supercapacitors and batteries. SPEs are light in weight, transparent, flexible and show good compatibility and interfacial contact between electrodes.

SPEs are made up of a polymer host, which consists of a macromolecule matrix of high molecular weight and electron donor groups containing sulfur, nitrogen and oxygen for coordination of ions providing spatial conformation to the doped alkali salt [9–13]. Host polymer must contain low glass transition temperature that can help in easy segmental motion of polymer chains, and with high dielectric constant, it helps in dissolution of salts [14]. When organic salts are added in a polymer system, due to the interaction of polar group in polymer system with cations of organic salts leads to dissociation of ions and travels along the chains of polymers through the hopping mechanism in amorphous phase occurred by the polymer [15]. Gel polymer electrolytes (GPEs) are third-generation polymer electrolytes which exhibit inert polymer matrix and carry both properties of solid-like rigid structure and liquid-like diffusive properties, provide better electrochemical window and best ionic conductivity [16, 17] and also provide high power density, cost-effective, and lightweight [18, 19]. The development of GPEs in rechargeable lithium polymer batteries has attracted much attention from past few decades because of their promising potential applications in electric vehicles and portable electronic devices and also exhibiting special advantages like high power density, long-lasting life cycle with improved safety conditions [20–22].

Many researchers worked with different host polymers such as poly(acrylonitrile) (PAN) [23], poly(vinylidene fluoride) (PVdF) [24] and poly(methyl methacrylate) (PMMA) [25]. PMMA is a synthetic polymer which is derived from monomer methyl methacrylate and is extensively used as host polymer in polymer electrolyte material due to its lightweight, high impact strength, less reactive toward electrolyte–electrode stability [26]. It has two electron-donating functional groups ($C=O$ and $O-CH_3$) which can easily coordinate with cation for complexation [27]. Many researchers have worked on different combinations of PMMA with different salts [28–33]. We report here first time SPE with a combination of PMMA and CH_3COOLi . Here, Li-ion conducting polymer electrolyte films were prepared using PMMA as host polymer and CH_3COOLi salt as dopant and both are dissolved in dimethyl formamide (DMF) in

order to get homogeneous solution by solution casting technique. Films with different ratios of PMMA and salt were prepared and characterized by X-ray diffraction (XRD) and Fourier-transform infrared spectroscopy (FTIR) for structural information. Optical absorption studies of films are carried out to find out the band gap of the material, and electrical conductivity studies are done for the feasibility of using these films in battery applications.

Experimental

Materials

Poly(methyl methacrylate) (PMMA) with molecular weight of $12 \times 10^5 \text{ g mol}^{-1}$ and lithium acetate (CH_3COOLi) were purchased from Sigma-Aldrich, and dimethyl formamide (DMF) is used as common solvent. All these chemicals are used directly without any further purification.

Polymer electrolyte preparation

PMMA is used as host polymer and CH_3COOLi salt as a dopant for complexation. PMMA and CH_3COOLi were kept under vacuum drying for the removal of excess moisture in the temperature range of $70 \text{ }^\circ\text{C}$ to $80 \text{ }^\circ\text{C}$ for about 24 h. Different ratios of PMMA + CH_3COOLi were prepared by varying the weight percents (60:40, 70:30, 80:20 wt%) using solution casting technique and used DMF as a common solvent. The solution was stirred for about 48 h till homogeneous solution was obtained. This solution was then poured into polypropylene dishes and left at room temperature for evaporation of solvent traces to get dry films.

Characterization

The prepared films were then subjected to different characterizations for further studies. X-ray diffraction (XRD) was used to study the phase of the material either crystalline or amorphous structure using XPERT-PRO diffractometer system with current 30 mA, and angle range is in between 10° and 90° . Fourier-transform infrared (FTIR) spectroscopy is used to identify functional group of material and also interaction between polymer and salt. FTIR spectra were recorded using Perkin-Elmer Alpha-E spectrophotometer. UV–visible spectroscopy is used to measure optical absorption of prepared samples by JASCO V-670 spectrophotometer of wavelength range 200–800 nm. AC conductivity studies are carried out for the prepared samples using HIOKI 3532-50 LCR HITESTER. Dielectric measurements were taken for the prepared solid polymer electrolyte films in the range of 42 Hz to 5 MHz using HIOKI 3532-50 LCR HITESTER [34].

Results and discussion

XRD analysis

The XRD pattern for the complexation of (PMMA:CH₃COOLi) with different wt% (pure PMMA, 80:20, 70:30, 60:40) is shown in Fig. 1. Pure PMMA of XRD graph has its characteristic peaks obtained at angles (2θ) $\sim 20^\circ$, where the peak is moderately sharp (diffused) due to semicrystalline nature of polymer, and there are no other remaining peaks which leads to weak in intensity toward higher angle side. The addition of Li salt concentration shifts the peak toward higher angle, and in (60:40) wt%, the peak has disappeared which confirms that the semicrystalline phase vanished and amorphous phase takes place which reveals us complexation has taken place between polymer matrix and cation of lithium salt (Li⁺).

FTIR analysis

Fourier-transform infrared spectroscopy (FTIR) reveals consistency of various functional groups in polymer and salt complexes. The significant change in stretching and bending vibrations of molecules is obtained in different wave number regions (cm⁻¹) with respect to various functional groups between the range of 400 and 4000 cm⁻¹. Different absorption intensities are studied by FTIR, and the spectra are recorded in transmittance mode (Table 1).

The FTIR spectra are recorded for different weight percentages of PMMA:CH₃COOLi (80:20, 70:30, 60:40) shown in Fig. 2. The absorption peaks

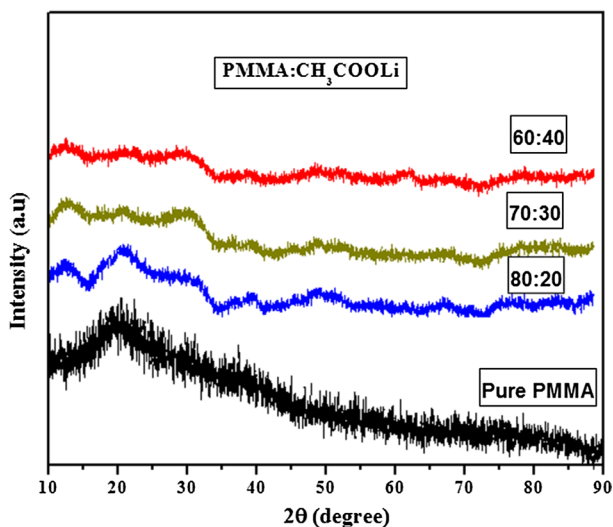


Fig. 1 XRD pattern for overlaid spectra of PMMA-based polymer electrolyte films for different ratios of PMMA:CH₃COOLi (pure PMMA, 80:20, 70:30, 60:40 wt%)

Table 1 Absorption features of FTIR spectra

Wave number (cm ⁻¹)	Modes of vibrations
752	C=O stretching
985	CH ₂ wagging
1148	CH ₂ twisting
1245	C–O stretching
1428	O–CH ₃ stretching
1730	C=O stretching
2949	C–H symmetric stretching

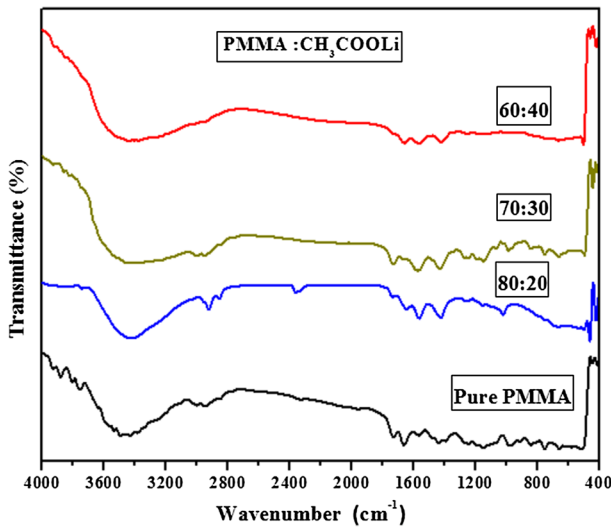


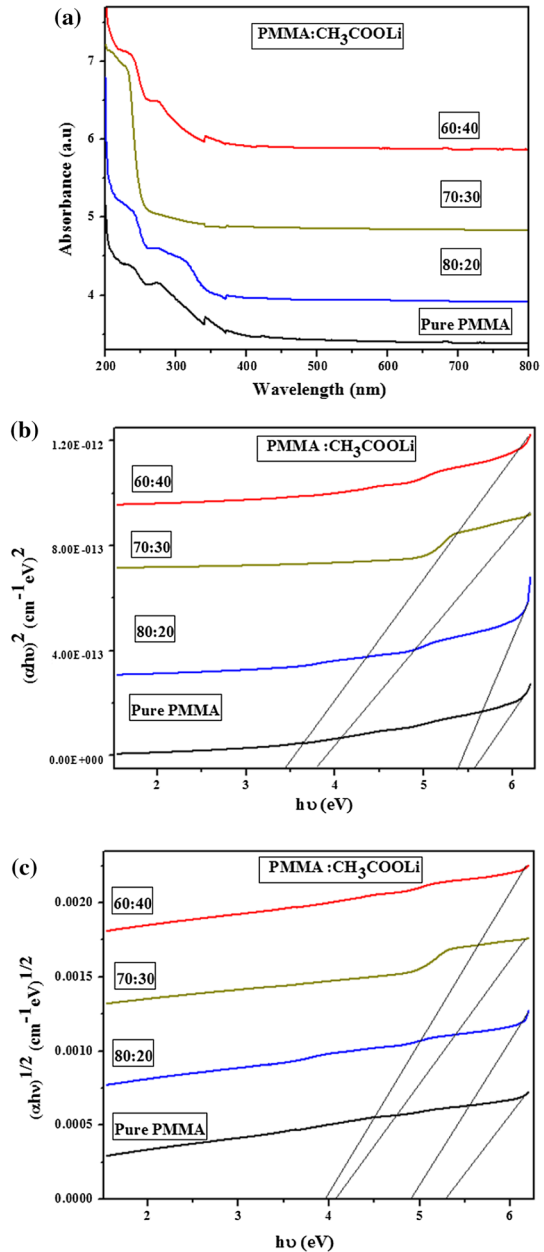
Fig. 2 FTIR pattern for overlaid spectra of polymer electrolyte films of different ratios PMMA:CH₃COOLi (pure PMMA, 80:20, 70:30, 60:40 wt%)

are observed at 752 cm⁻¹ due to CH₂ rocking vibrations. The absorption peaks at 2949 cm⁻¹ and 1245 cm⁻¹ are obtained for C–H symmetric stretching. The strong absorption peak is observed at 1730 cm⁻¹ due to C=O stretching by carbonyl group. A broad peak is obtained in between 3400 and 3700 cm⁻¹ due to OH functional group. The vibration frequencies at 1428, 1148 and 985 cm⁻¹ are assigned to O–CH₃ stretching, CH₂ twisting and CH₂ wagging, respectively. FTIR confirmed the broadening and shifting of absorption peaks due to the interaction of salt with polymer [35].

UV–visible absorption studies

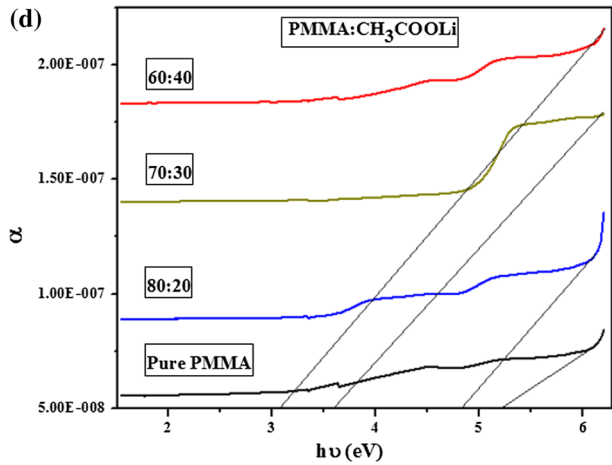
UV–visible spectra for PMMA:CH₃COOLi of different ratios (pure PMMA, 80:20,70:30,60:40) are shown in Fig. 3a, and the wavelength range is from 200 to

Fig. 3 **a** UV–visible spectra for polymer electrolyte films of different ratios PMMA:CH₃COOLi (pure PMMA, 80:20, 70:30, 60:40 wt%). **b** Direct energy band gap graph for different ratios of polymer electrolyte films PMMA:CH₃COOLi (pure PMMA, 80:20, 70:30, 60:40 wt%). **c** Indirect energy band gap graph for different ratios of polymer electrolyte films of PMMA:CH₃COOLi (pure PMMA, 80:20, 70:30, 60:40 wt%). **d** Absorption edge graph for different ratios of polymer electrolyte films PMMA:CH₃COOLi (pure PMMA, 80:20, 70:30, 60:40 wt%)



800 nm. The plot clearly shows that for pure PMMA there is a sharp decrease in absorption around 220–280 nm around UV region which is mostly due to $\pi-\pi^*$ transitions as there is an increase in salt (CH₃COOLi) ratio [35], and it is shifted toward the longer wavelength which shows better absorption. The shifting toward longer wavelength indicates small band gap for the (PMMA+Li salt) samples.

Fig. 3 (continued)



PMMA:CH₃COOLi (60:40) sample has got larger absorption, so this strong shift indicates the addition of Li salt concentration caped on the polar group of the polymer chain due to π -delocalization. So as salt percentage increases, absorption increases which indicates the occurrence of electronic interaction between pure PMMA polymer and Li salt concentration. Optical analysis is a simple and direct method to measure optical band gap of materials in absorption spectrum in transmitting radiation. A photon of certain energy excites an electron from lower to higher energy level during absorption process. In transmitted radiation, the number of possible transitions by which an electron absorbs energy and can make transitions from fundamental energy level to rapid rising to band-to-band transitions is known as absorption edge where optical energy band gap is determined. Based on materials, band gap is divided into two types. When the valence band and conduction band are equal, the crystal momentum is zero to be considered as direct band gap. When the valence band and conduction band are not equal, the crystal momentum is nonzero to be considered as indirect band gap [36]. The direct band gap, indirect band gap and absorption edge values are shown in Table 2.

To calculate energy band gap values for polymer electrolyte films PMMA:CH₃COOLi with different compositions (PMMA, 80:20, 70:30 and 60:40), the absorption graphs were plotted between absorption coefficient $(\alpha h\nu)^{1/2}$, $(\alpha h\nu)^2$ and (α) as a function of photon energy ($h\nu$). From the UV–visible spectra, the optical energy band gap is derived from Tauc’s plot which can be determined by translation of spectra. The absorption coefficient value is given by

$$\alpha(h\nu) = K [h\nu - E_g]^n \tag{1}$$

where ‘ α ’ is the absorption coefficient which is determined by photon energy function using this equation

$$\alpha = 2.303(A/t) \tag{2}$$

where from Eqs. (1) and (2) ‘ h ’ is the Planck’s constant, ‘ K ’ is the constant depending on structure of specimen, ‘ ν ’ is the incident light frequency, ‘ E_g ’ is the energy

Table 2 Optical energy band gap values for PMMA-based polymer electrolyte films

PMMA-based polymer electrolyte films	Optical energy band gap		E_g (eV)
	Direct band gap (eV)	Indirect band gap (eV)	
Pure PMMA	5.5	5.29	5.21
PMMA:CH ₃ COOLi (80:20)	5.36	4.90	4.84
PMMA:CH ₃ COOLi (70:30)	3.80	4.08	3.61
PMMA:CH ₃ COOLi (60:40)	3.50	3.61	3.06

Bold fonts were used to highlight the results

band gap between bottom of conduction band and top of valence band, ' t ' is the thickness of sample and ' A ' is the absorbance. For different compositions of polymer electrolyte (pure PMMA, 80:20, 70:30, 60:40), energy band gap values are obtained from both direct, indirect and absorption edge. From Fig. 3b, c, the energy band gap values are calculated and shown in Table 2. It is observed that increasing salt concentration leads to decrease in band gap energy. The addition of salt concentration influences the decrease in activation energy in polymer chain such that existence of local cross-linking between the polymer host and salt will be developed within the amorphous phase. This confirms the compatibility between polymer host and salt [27]. By increasing the salt composition ratio, there is a decrease in energy band gap. From Fig. 3a, we observe that there is a strong absorption in UV region and transmission in the visible region. So wide band gap has reduced to narrow energy band gap and the new material having small band gap and good film formation leads to cost-effective and flexible. From these particular observations, we can conclude that this polymer electrolyte film with low band gap is useful for coatings in both optical and electronic devices [36].

In the present work, the direct band gap value for pure PMMA is 5.5 eV which is reduced to 3.50 eV in the case of 60:40 wt% of PMMA + CH₃COOLi. When compared with the literature value, we observed the lowest direct band gap value of 3.50 eV by adding lithium salt since lithium salt is lightweight, has small ionic radius and also is one of the active charge carriers that can hop in a polymer chain which helps in increasing the polymer conductivity. Lithium salt also promotes better direct transition from valence band to conduction band. Generally in polymeric materials, absorption of light takes place in both UV and visible regions and the electronic transitions can happen due to σ , π and n-orbitals and it is explained by molecular orbital theory. The electronic transitions involved in both UV and visible regions especially from 150 to 250 nm are due to $n \rightarrow \sigma^*$ transitions; from 200 to 400 nm, it is due to $\pi \rightarrow \pi^*$ transitions; and from 400 to 700, it is due to $n \rightarrow \pi^*$ transitions. In the present work, we observed a sharp decrease in the absorption for pure PMMA with increasing salt (CH₃COOLi) ratio around 220–280 nm which is due to $\pi \rightarrow \pi^*$ transitions related to carbonyl group (C=O) [38].

Refractive index and optical dielectric loss study

The calculation of refractive index within the definite range of wavelength (from near infrared to ultraviolet) is important as it is useful in thin-film investigation and finds in diverse applications. Refractive index (n) is calculated by using the formula,

$$E_g = 95 \text{ eV}/n^4 \tag{3}$$

where E_g is the energy band gap. This formula is applicable for solids [39] Optical dielectric loss is calculated by using the following relation,

$$\epsilon_i = 2 \times n \times k \tag{4}$$

where n is the refractive index and k is the extinction coefficient as a function of wavelength, $k = \alpha\lambda/4\pi$. Figure 4 shows variation of the optical dielectric loss with wavelength. The pattern of dielectric loss for pure PMMA shows a sharp decrease at absorption edge and continues to be constant as wavelength increases. The PMMA+Li salt-doped samples show similar behavior, but there is shift at longer wavelength for the doped samples compared to pure PMMA. It is clear that the optical band gap values obtained from dielectric loss (Fig. 4) are similar to the E_g values obtained from Table 2 (Tauc’s plot values) (Table 3). The optical band gap values of PMMA+Li salt-doped samples are shown in Table 4.

Thus, the type of electronic transition which takes place is direct transition in pure PMMA whereas forbidden direct transition in the case of PMMA:CH₃COOLi (60:40,70:30,80:20) samples. Hence, the dielectric loss studies are used for calculating optical band gap values. In the present work, we observed the lowest optical band gap in the case of PMMA:CH₃COOLi (60:40 wt%) compared with the

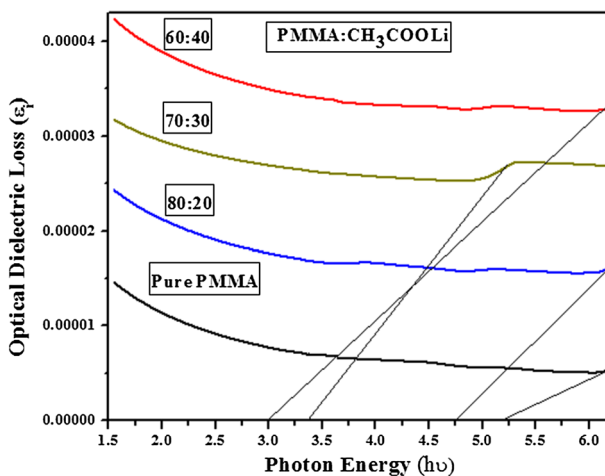


Fig. 4 Optical dielectric loss versus photon energy ($h\nu$) for pure PMMA and doped PMMA:CH₃COOLi samples

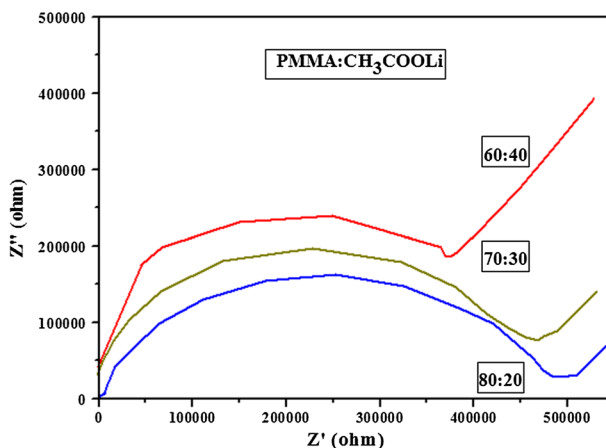
Table 3 Comparison table for optical band gap values with the literature

Sample description	Optical band gap from Tauc's model (eV)		Reference
	Pure PMMA	Doped PMMA with different wt%	
PMMA + CuS nanoparticles (0, 2, 4, 6 and 8 wt%)	5.05	CuS nanoparticles (8 wt%), 3.95 eV	[37]
PMMA + GT extracts (0, 14 and 28 mL)	4.9	GT extracts (28 mL), 2.6 eV	[38]
PMMA + CH₃COOLi (100:0, 80:20, 70:30 and 60:40 wt%)	5.5	60:40 (wt%), 3.50 eV	Present work

Bold fonts were used to highlight the results

Table 4 Comparison table for optical dielectric loss and Tauc's plot values

Sample description	Optical dielectric loss plot [E_g] eV	Tauc's plot [E_g] eV
Pure PMMA	5.2	5.21
PMMA:CH ₃ COOLi (80:20)	4.7	4.84
PMMA:CH ₃ COOLi (70:30)	3.3	3.61
PMMA:CH ₃ COOLi (60:40)	3.0	3.06

**Fig. 5** AC conductivity graph for different ratios of polymer electrolyte films of PMMA:CH₃COOLi (80:20, 70:30, 60:40 wt%)

literature values. Hence, this material could be potential candidate for the application in optical devices (Fig. 5).

Conductivity studies

The conductivity studies of polymer electrolyte films have been done using complex impedance spectroscopy (CIS) analysis. At room temperature, typical

Nyquist plots were drawn for different compositions of polymer electrolytic films (PMMA:CH₃COOLi). The complex impedance spectroscopy reveals a high-frequency semicircular arc which follows toward lower-frequency region with a spike at room temperature. An expanded semicircle is acquired because of frequency-dependent (C_p) parallel capacitor to the bulk resistor. The point of intersection of semicircle to the real axis obtains the value of bulk resistance (R_b). The conductivity spectra of solid polymer electrolytes exhibit semicircular arc at low frequency which reveals that the flow of majority charge carriers through bulk distribution is mostly due to ions which enhances the conductivity. It corresponds to good contact between electrolyte and electrode interphase during polarization phenomenon. The cole–cole plots were drawn between real part Z' and imaginary part Z'' , and from this, ionic conductivity is calculated by using a relation:

$$\sigma_{ac} = d / (R_b * A) \quad (5)$$

where ‘ d ’ is the thickness of the sample, ‘ A ’ is the area of electrolyte and ‘ R_b ’ is the bulk resistance.

Using Eq. (5), the ionic conductivity values of polymer electrolytes for different compositions (80:20, 70:30, 60:40) are obtained. The ionic conductivity value of pure PMMA value is obtained from the literature as (10^{-16} S/cm) at room temperature ($T=30$ °C). By increasing the salt concentration, crystallinity vanishes and leads to amorphous phase where ions mobility is easier; therefore, the increase in conductivity is observed. The conductivity values are obtained as shown in Table 5. Pure PMMA ionic conductivity is 10^{-16} S/cm. When it is complexed with salt PMMA:CH₃COOLi (60:40 wt%), ionic conductivity is increased to 10^{-5} S/cm which is an excellent enhancement in ionic conductivity at room temperature when compared to the reported literature [27].

When compared to different combinations of polymer electrolytes with different blends, lithium salts and plasticizers, we obtained better conductivity result 8.21×10^{-5} S/cm for PMMA:CH₃COOLi (60:40 wt%) (Table 6).

Comparison between AC and DC conductivity studies

From Fig. 6a–c plotted between frequency (Hz) and σ_{ac} (S/cm), the plateau region which is constant can be considered as DC conductivity. Hence, DC conductivity can be obtained from AC conductivity plots as it is shown in correlation Table 7.

Table 5 AC conductivity values for PMMA-based polymer electrolyte films

Polymer electrolyte films (PMMA:CH ₃ COOLi) (wt%)	AC conductivity value at room temperature ($T=30$ °C) (S/cm)
80:20	5.98×10^{-7}
70:30	6.65×10^{-7}
60:40	8.21×10^{-5}

Table 6 Comparison table of conductivity values for PMMA-based polymer electrolytes

S. no.	Combination of polymer electrolytes	Conductivity (σ) S/cm	References
1	PMMA–LiClO ₄	6.07×10^{-9}	[27]
2	MG49–PMMA–LiClO ₄ MG49–PMMA–LiBF ₄	1.5×10^{-08} 8.6×10^{-06}	[40]
3	PMMA–Li ₂ SO ₄ –DBP–ZrO ₂	0.13×10^{-6}	[41]
4	PMMA–CH₃COOLi	8.21×10^{-5}	Present work

Bold fonts were used to highlight the results

DC conductivity studies Figure 6d represents temperature dependence of DC conductivity for PMMA:CH₃COOLi (80:20, 70:30, 60:40 wt%) samples. It shows that there is an increase in conductivity as temperature increases. DC conductivity plots obey Arrhenius relationship

$$\sigma_{dc} = \sigma_0 \exp(-E_a/KT) \quad (6)$$

where σ_0 is the pre-exponential factor, E_a is the activation energy, K is the Boltzmann constant and T is the absolute temperature. DC conductivity is calculated by using the formula

$$\sigma_{dc} = iL/VA \quad (7)$$

where i is the current, L is the thickness of the sample, V is the applied constant voltage and A is the area of the sample.

From Fig. 4d, it is observed that temperature and conductivity are directly proportional and it may lead to decrease in viscosity, and then, chain flexibility takes place. Charge carriers can hop in the polymer chain which results in enhancing the conductivity and can be explained by free volume model. Hence, conductivity increases with increasing the Li salt concentration [42, 43].

Dielectric analysis

The dielectric spectroscopy is carried out to measure the electrical properties of prepared films. This analysis was done by Hioki 3532-50 LCR HITESTER between 42 HZ and 1 MHZ range. Dielectric permittivity is characterized by $\epsilon^*(\omega) = \epsilon' - j\epsilon''$ where ϵ' and ϵ'' are the real (dielectric constant) and imaginary (dielectric loss) parts. Figure 7a, b gives the values of real and imaginary parts of dielectric permittivity at room temperature. It is clear that high ϵ' and ϵ'' values are obtained at low frequencies. At low frequencies, the dipoles will be able to align in the direction of the field due to polarization phenomenon and also reveal that by decreasing frequency, there is a sharp increase in dielectric constant which leads to increasing the values of ϵ' and ϵ'' . At moderate frequencies, dipoles will not be able to align in the field direction which leads to decreasing the values of ϵ' and ϵ'' . At high frequencies, in the applied field direction the dipoles cannot orient themselves. As frequency increases in the applied electric field direction, there is no excess ion diffusion in the direction of field between the

Fig. 6 a–c Plots between frequency and AC conductivity (σ_{ac}) for different ratios of PMMA:CH₃COOLi (80:20, 70:30 and 60:40 wt%) polymer electrolytes. **d** Plots of $\log \sigma_{dc}$ versus $1000/T$ for PMMA:CH₃COOLi (80:20, 70:30, 60:40 wt%) samples

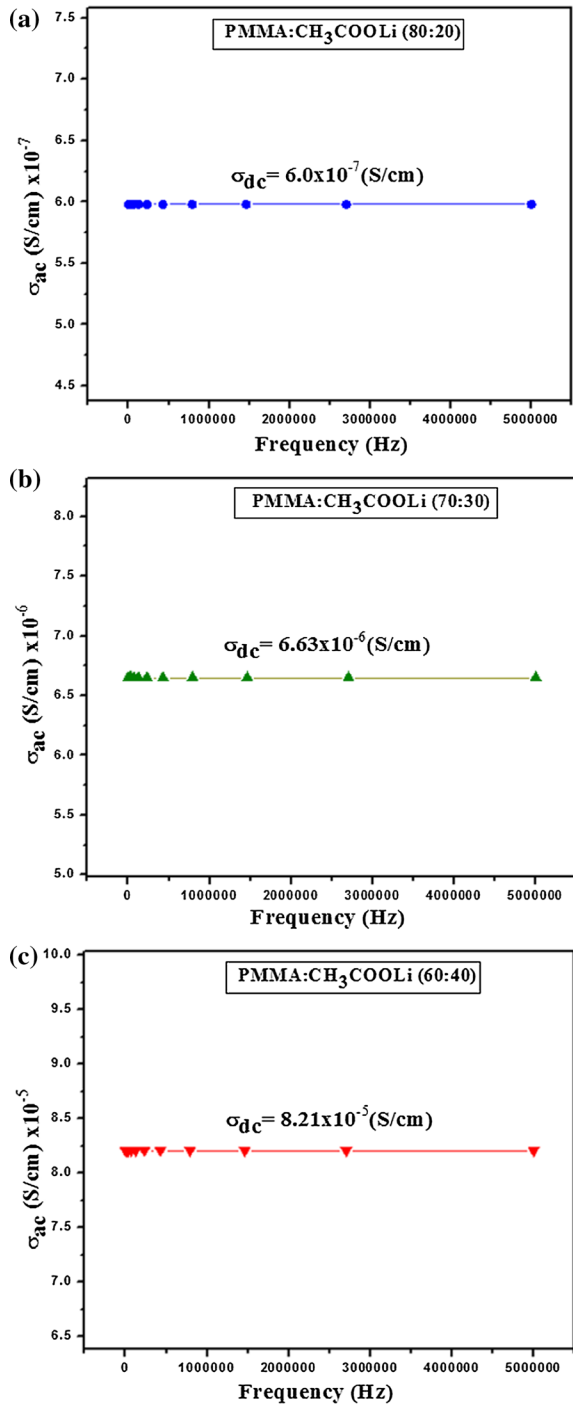
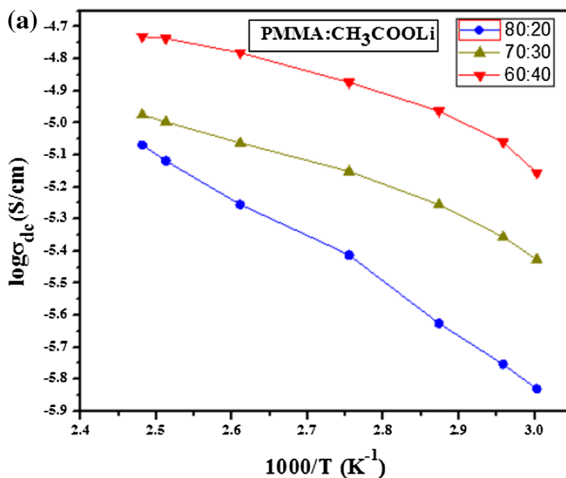


Fig. 6 (continued)

**Table 7** Correlation table between AC conductivity and DC conductivity

PMMA:CH ₃ COOLi polymer electrolytes (wt%)	DC conductivity values obtained from AC plots (S/cm)	DC conductivity values (S/cm)
PMMA:CH ₃ COOLi (80:20)	6.0×10^{-7}	3.651×10^{-6}
PMMA:CH ₃ COOLi (70:30)	6.63×10^{-6}	6.685×10^{-6}
PMMA:CH ₃ COOLi (60:40)	8.21×10^{-5}	1.259×10^{-5}

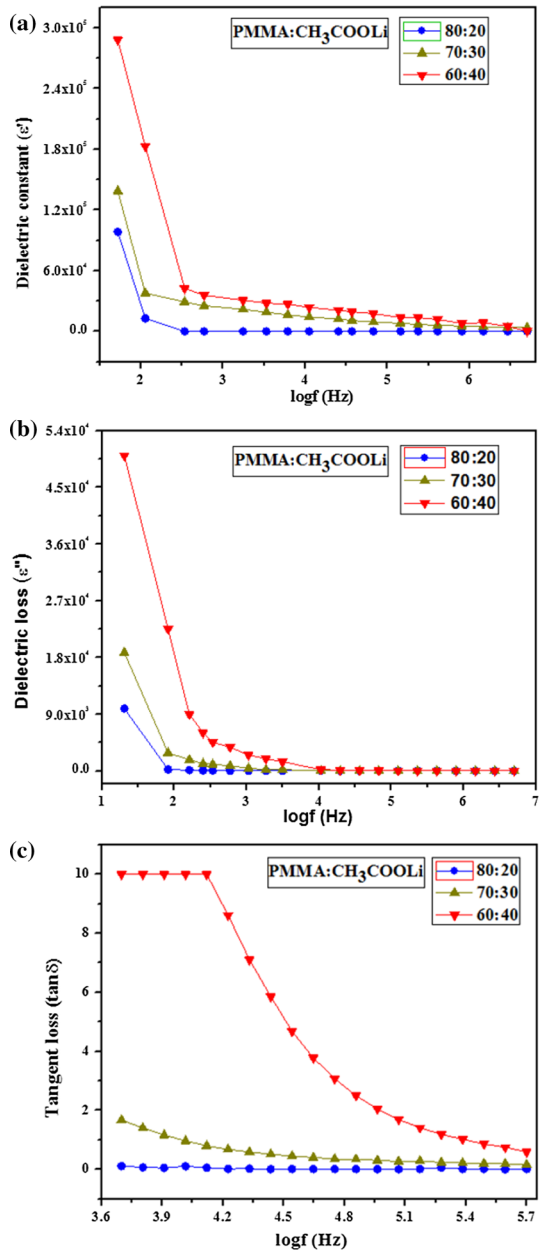
electrode and electrolyte interface which leads to much decrease in ϵ' and ϵ'' [44].

From Fig. 7c, it shows the relation between dielectric loss tangent ($\tan\delta$) and $\log F$ for various ratios of polymer electrolyte films. In all samples, it is observed that there is a decrease in dielectric tangent loss while increasing frequency due to the occurrence of relaxing dipoles. As we increase the salt concentration for pure PMMA, the tangent loss shifts toward the higher-frequency side. This confirms that there is a decrease in relaxation time which leads to an increase in conductivity through the motion of ions in polymer [44].

Electric modulus analysis

An electric modulus spectrum is useful for understanding the transport process, hopping mechanism and type of charge carriers which exist in an ionic conducting polymer electrolyte. It is especially used to examine the relaxation process in solid polymer electrolytes and ceramic materials through electrical response of those materials. The long-range conduction can be investigated through complex electric modulus which includes both impedance and permittivity. There are two parts in electric modulus (M' and M'') where M' represents real modulus and M'' represents imaginary

Fig. 7 **a** Real part of dielectric constant (ϵ') versus frequency for different ratios of polymer electrolyte films PMMA:CH₃COOLi (80:20, 70:30, 60:40 wt%) at room temperature (303 K). **b** Imaginary part of dielectric constant (ϵ'') versus frequency for different ratios of polymer electrolyte films PMMA:CH₃COOLi (80:20, 70:30, 60:40 wt%) at room temperature (303 K). **c** Plots of tangent loss (tan δ) versus log f of PMMA:CH₃COOLi (80:20, 70:30, 60:40 wt%) polymer electrolyte films



modulus. As per the formula, we know that electric modulus is reciprocal of relative permittivity and it is proved from Fig. 8a, b. The following formula is obtained as $M^* = 1/\epsilon^*$; $M^* = M' + M'' = 1/\epsilon' - j\epsilon'' = \epsilon'/(\epsilon'^2 + \epsilon''^2) + j\epsilon''/(\epsilon'^2 + \epsilon''^2)$

$$M^* = j\omega c_0 z^* = \omega c_0 z' + j\omega c_0 z''.$$

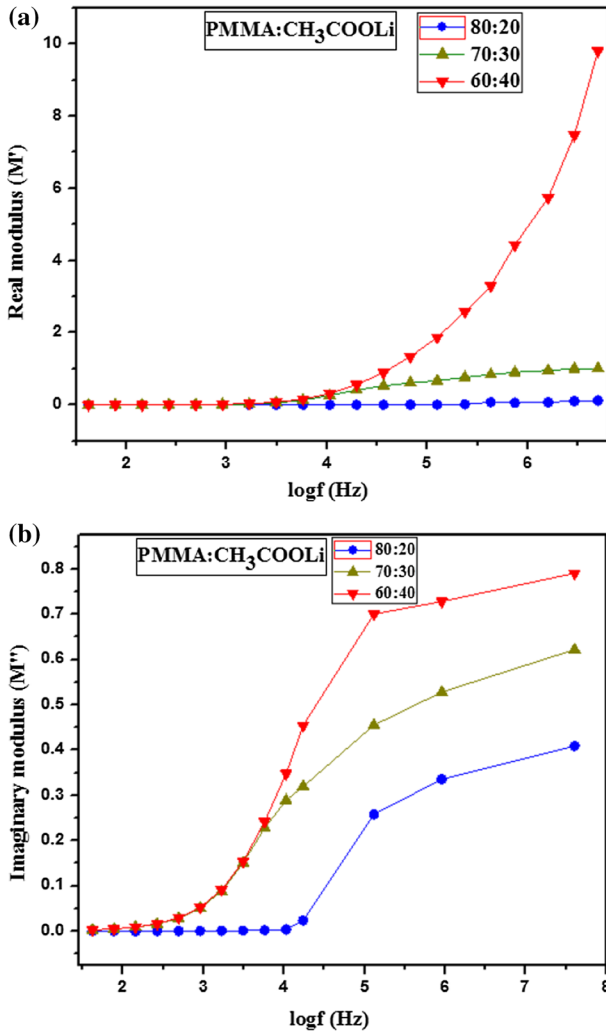


Fig. 8 **a** Real modulus (M') versus $\log f$ of PMMA:CH₃COOLi (80:20, 70:30, 60:40 wt%) polymer electrolyte films. **b** Imaginary modulus (M'') versus $\log f$ of PMMA:CH₃COOLi (80:20, 70:30, 60:40 wt%) polymer electrolyte films

From the above equation, electric modulus is reciprocal of complex relative permittivity and it is useful to study the electrical relaxation process. Figure 8a, b represents dielectric modulus versus $\log f$ where different spectra for both real (M') and imaginary (M'') electric modulus are plotted for different ratios of solid polymer electrolyte films at room temperature. From Fig. 8a, the M' values at low frequencies are very low and approaches to zero due to the shifting of electrode polarization contribution. As we observe that if frequency increases, M' also increases. As the salt concentration increases, the spectra are transferred toward the higher-frequency

region which resembles dispersion region. There is a change in shape of the peak due to long-range conductivity relaxation process. From this particular phenomenon, we conclude that there is a scope for excellent electrochemical stability; therefore, it can be used in battery application.

Figure 8b shows that as frequency increases, M'' also increases. This is due to hopping of ions in polymer electrolyte film which reaches to maximum value at one particular frequency. A peak is observed at this frequency which shows that the material is having ionic conductivity. As frequency increases, M'' also increases due to charge carriers which are confined within the potential. From these graphs, we can also calculate relaxation time τ and using the formula $2\pi f_{\max}\tau = 1$ where f_{\max} corresponds to M''_{\max} [45].

Conclusions

In this work, a novel solid polymer electrolyte (SPE) films were prepared with different weight compositions (PMMA:CH₃COOLi) (pure PMMA, 80:20, 70:30, 60:40 wt%) using solution casting technique. XRD analysis confirmed that the complexation has taken place and observed the amorphous nature in the SPE films. FTIR analysis further confirmed the complexation between polymer and salt due to the appearance of new peaks in the SPE films. From UV–visible studies, with increasing salt concentration in SPEs, energy band gap value decreased from 5.21 to 3.06 eV. AC impedance studies showed the highest value of ionic conductivity 8.21×10^{-5} S/cm at 303 K for the SPE film PMMA:CH₃COOLi (60:40 wt%) compared to the reported literature. Dielectric measurements were taken for the different SPEs, and as frequency decreases, the dielectric permittivity increases due to polarization effect. The prepared SPE exhibits high ionic conductivity, and thus, SPE has great potential application for all solid-state batteries at room temperature.

Acknowledgements The authors would like to thank the management, Koneru Lakshmaiah Education Foundation (KLEF), for providing kind support for our work. K. Sravanthi is thankful to Dr K. Swapna for UV–visible spectroscopy measurements.

References

1. Qingqing Z, Kai L, Fei D, Xingjiang L (2017) Recent advances in solid polymer electrolytes for lithium batteries. *Nano Res* 10:4139–4174
2. Scrosati B (2000) Recent advances in lithium ion battery materials. *Electrochim Acta* 45:2461–2466
3. Stephan AM (2006) Review on gel polymer electrolytes for lithium batteries. *Eur Polym J* 42:21–42
4. Ahmad S (2009) Polymer electrolytes: characteristics and peculiarities. *Ionics* 15:309–321
5. Abraham KM, Jiang Z, Carroll B (1997) Highly conductive PEO-like polymer electrolytes. *Chem Mater* 9:1978–1988
6. Li Z, Huang J, Liaw BY, Metzler V, Zhang J (2014) A review of lithium deposition in lithium-ion and lithium metal secondary batteries. *J Power Sources* 254:168–182

7. Kang X (2004) Non-aqueous liquid electrolytes for lithium-based rechargeable batteries. *Chem Rev* 104:4303–4418
8. Armand M (1983) Polymer solid electrolytes—an overview. *Solid State Ion* 9:745–754
9. Anil A, Sharma AL (2017) Polymer electrolytes for lithium ion batteries: a critical study. *Ionics* 23:497–540
10. Kalhoff J, Eshetu GG, Bresser D, Passerini S (2015) Safer electrolytes for lithium-ion batteries: state of the art and perspectives. *Chem Sus Chem* 821:54–75
11. Marcinek M et al (2015) Electrolytes for Li-ion transport—review. *Solid State Ion* 276:107–126
12. Baskakova YV, Yarmolenko OV, Efimov ON (2012) Polymer gel electrolytes for lithium batteries. *Russ Chem Rev* 81:367–380
13. Berthier C, Gorecki W, Minier M, Armand MB, Chabagno JM, Rigaud P (1983) Microscopic investigation of ionic conductivity in alkali metal salts-poly(ethylene oxide) adducts. *Solid State Ion* 11:91–95
14. Cui Y, Xinmiao L, Jingchao C, Zili C, Qinglei W, Weisheng H, Xiaochen L, Zhihong L, Guanglei C, Jiwen F (2017) Facile and reliable in situ polymerization of poly(ethyl cyanoacrylate)-based polymer electrolytes toward flexible lithium batteries. *Appl Mater Interfaces* 9:8737–8741
15. Jeddi K, Qazvini NT, Jafari SH, Khonakdar HA (2010) Enhanced ionic conductivity in PEO/PMMA glassy miscible blends: role of nano-confinement of minority component chains. *J Polym Sci B Polym Phys* 48:2065–2071
16. Sequeira C, Santos D (2010) *Polymer electrolytes fundamentals and applications*. Elsevier, Amsterdam
17. Hellio D, Djabourov MP (2006) Physically and chemically cross linked gelatin gels. *Macromol Symp* 241:23–27
18. Armand M, Tarascon JM (2008) Building better batteries. *Nature* 451:652–657
19. Song JY, Wang YY, Wan CC (1999) Review of gel-type polymer electrolytes for lithium-ion batteries. *J Power Sources* 77:183–197
20. Rao M, Geng X, Liao Y, Hu S, Li W (2012) Preparation and performance of gel polymer electrolyte based on electrospun polymer membrane and ionic liquid for lithium ion battery. *J Membr Sci* 37:399–400
21. Kim JK, Shin CR, Ahn JH, Matic A, Jacobsson P (2011) Highly porous LiMnPO₄ in combination with an ionic liquid-based polymer gel electrolyte for lithium batteries. *Electrochem Commun* 13:1105–1108
22. Stephan AM, Nahm KS, Kulandainathan MA, Ravi G, Wilson J (2006) Poly(vinylidene fluoride-hexafluoropropylene) (PVdF-HFP) based composite electrolytes for lithium batteries. *Eur Polym J* 42:1728–1734
23. Alamgir M, Abraham KM (1993) Li ion conductive electrolytes based on poly(vinyl chloride). *J Electrochem Soc* 140:96
24. Saito Y, Capigila C, Yamamoto H, Mustarelli P (2000) Ionic conduction mechanisms of polyvinylidene fluoride-hexafluoropropylene type polymer electrolytes with LiN(CF₃SO₂)₂. *J Electrochem Soc* 147:1645
25. Panero S, Scrosati B (2000) Gelification of liquid-polymer systems: a valid approach for the development of various types of polymer electrolyte membranes. *J Power Sources* 90:13–19
26. Malcom P, Stevens P (2000) Polymer chemistry: an introduction. *J Chem Educ* 77:167–176
27. Shukla N, Thakur AK (2009) Role of salt concentration on conductivity optimization and structural phase separation in a solid polymer electrolyte based on PMMA-LiClO₄. *Ionics* 15:357–367
28. Appetecchi GB, Croce F, Scrosati B (1995) Kinetics and stability of the lithium electrode in poly(methylmethacrylate)-based gel electrolytes. *Electrochim Acta* 40:991–997
29. Bohnke O, Frand G, Rezzani M, Rousselot C, Truche C (1993) Fast ion transport in new lithium electrolytes gelled with PMMA-influence of polymer concentration. *Solid State Ion* 66:97–104
30. Wiczczonek W, Stevens JR (1997) Impedance spectroscopy and phase structure of polyether-Poly(methyl methacrylate)-LiCF₃SO₃ blend-based electrolytes. *J Phys Chem B* 101:1529–1534
31. Ali AMM, Yahya MZA, Bahron H, Subban RHY, Harun MK, Atan I (2007) Impedance studies on plasticized PMMA-LiX [X: CF₃SO₃⁻, N(CF₃SO₂)₂⁻] polymer electrolytes. *Mater Lett* 61:2026–2029
32. Rajendran S, Uma T (2000) Characterization of plasticized PMMA-LiBF₄ based solid polymer electrolytes. *Bull Mater Sci* 2:27–29
33. Chen HW, Lin TP, Chang FC (2002) Ionic conductivity enhancement of the plasticized PMMA/LiClO₄ polymer nano composite electrolyte containing clay. *Polymer* 43:5281–5288

34. Senthil J, Nagarajan G, Neyvasagam K (2015) FTIR and ionic conductivity studies on PMMA based gel polymer electrolytes. *Int J Enhanc Res Sci Technol Eng* 4:76–80
35. ShahenoorBasha SK, SunitaSundari G, Vijay Kumar K, Rao MC (2017) Optical and dielectric properties of PVP based composite polymer electrolyte films. *Polym Sci Ser A* 59:554–565
36. Abdelrazek EM, Hezma AM, El-khodary A, Elzayat AM (2016) Spectroscopic studies and thermal properties of PCL/PMMA biopolymer blend. *Egypt J Basic Appl Sci* 3:10–15
37. Aziz Shujahadeen B, Abdulwahid Rebar T, Rsaul Hazhar A, Ahmed Hameed M (2016) In situ synthesis of CuS nanoparticle with a distinguishable SPR peak in NIR region. *J Mater Sci Mater Electron* 27:4163–4171
38. Aziz SB, Abdullah OG, Hussein AM, Ahmed HM (2017) From insulating PMMA polymer to conjugated double bond behavior: green chemistry as a novel approach to fabricate small band gap polymers. *Polymers* 9:626
39. Ravindra NM, Ganapathy P, Choi J (2007) Energy gap–refractive index relations in semiconductors—an overview. *Infrared Phys Technol* 50:21–29
40. Su'ait MS, Ahmada A, Hamzaha H, Rahman MYA (2011) Effect of lithium salt concentrations on blended 49% poly(methyl methacrylate) grafted natural rubber and poly(methyl methacrylate) based solid polymer electrolyte. *Electrochim Acta* 57:123–131
41. Uma T, Mahalingam T, Stimming U (2003) Mixed phase solid polymer electrolytes based on poly(methylmethacrylate) systems. *Mater Chem Phys* 82:478–483
42. Aziz Shujahadeen B, Rasheed Mariwan A, Hussein Ahang M, Ahmed Hameed M (2017) Fabrication of polymer blend composites based on [PVA-PVP](1 - x):(Ag₂S)x(0.01 ≤ x ≤ 0.03) with small optical band gaps: structural and optical Properties. *Mater Sci Semicond Process* 71:197–203
43. Krishna Jyothi N, Vijaya Kumar K, Sunita Sundari G, Narayana Murthy P (2016) Ionic conductivity and battery characteristic studies of a new PAN-based Na⁺ ion conducting gel polymer electrolyte system. *Indian J Phys* 90:289–296
44. Gurusiddappa J, Madhuri W, Padma Suvarna R, Priya Dasan K (2016) Conductivity and dielectric behavior of polyethylene oxide-lithium perchlorate solid polymer electrolyte films. *Indian J Adv Chem Sci* 4:4–19
45. Anil A, Sharma AL, Kumar Dinesh, Sadiq M (2016) Structural and dielectric behaviour of blend polymer electrolyte based on PEO-PAN + LiPF₆. *Asian J Eng Appl Technol* 5:4–7

Publisher's Note Springer Nature remains neutral with regard to jurisdictional claims in published maps and institutional affiliations.